



Original scientific paper

***Pouteria sapota* as green CO₂-corrosion inhibition of carbon steel**

Guillermo Salinas-Solano¹, Jesus Porcayo-Calderon², Ana Karen Larios-Galvez¹ and Jose Gonzalo Gonzalez-Rodriguez^{1,✉}

¹Universidad Autonoma del Estado de Morelos, Centro de Investigación en Ingeniería y Ciencias Aplicadas, Av. Universidad 1001, 62209-Cuernavaca, Morelos, Mexico

²Universidad del Estado de Sonora, Departamento de Ingeniería Química y Metalúrgica, Hermosillo, Sonora 83000, Mexico

Corresponding author: ✉ ggonzalez@uaem.mx; Tel: 52777 3297084

Received: October 21, 2021; Accepted: January 21, 2022; Published: January 31, 2022

Abstract

Imidazoline obtained from the essential oil contained in *Pouteria sapota* seed was tested as an environmentally-friendly corrosion inhibitor of 1018 carbon steel in a CO₂ saturated 3.5 % NaCl solution using electrochemical techniques. This imidazoline contains fatty acids with long hydrophobic chains, with 52.73 % of unsaturated (oleic and linolenic acids) and 40 % of saturated (palmitic and myristic acids) compounds. Polarization curves revealed that this inhibitor is a highly efficient mixed-type of inhibitor with the inhibitor efficiency of 99.9 % reached at 25 ppm. Also, the lowest pitting potential value was observed at 25 ppm of inhibitor, making the carbon steel highly susceptible to the pitting type of corrosion. Corrosion current density value decreased by nearly four orders of magnitude, and a passive film formation was induced for inhibitor concentrations higher than 5 ppm. Accordingly, polarization resistance values were increased from 100 Ω cm² up to about 10⁶ Ω cm² at 25 ppm of inhibitor. The inhibitor forms a protective film of corrosion products adsorbed on the metal surface in a very strong chemical way, following a Langmuir type of adsorption isotherm. This was supported by electrochemical impedance spectra that showed two relaxation processes ascribed to electrode interface and film regions. In agreement with polarization resistance data, the total electrode resistance determined by interfacial charge transfer and film resistance increased up to 8.2 × 10⁵ Ω cm² in the presence of 25 ppm of inhibitor. SEM images additionally showed that type of corrosion was fully changed from uniform to a localized type when 25 ppm of inhibitor was added into the solution.

Keywords

Acid corrosion; naturally occurring inhibitor; electrochemical impedance

Introduction

The presence of water in the oil and gas field, together with high content of CO₂, acetic acid, and H₂S, has increased the corrosion rate of involved metals [1,2]. One of such involved metals is carbon steel, which is extensively used in the oil industry as the most common material for tubing. One of the most frequently used methods to mitigate CO₂-corrosion is by applying organic inhibitors, where the presence of heteroatoms including phosphorus, nitrogen, sulfur and carbon protects steel surface by forming a barrier of corrosion products. In such a way, metals are protected from the action of the environment [3-10]. However, due to serious environmental concerns, a lot of research concerning less toxic, cheaper, and more environmentally friendly compounds has been undertaken in the last years [11-13]. Thus, *Allium cepa* [11], expired drugs [14-18], *Thymbra capitata* [15], amino surfactants and imidazolines obtained from palm, avocado and rice bran oil [13,19,20] were already evaluated as corrosion inhibitors for iron and steel in different media. Abdallah *et al.* [12] evaluated natural nutmeg oil as a green inhibitor for carbon steel in 1.0 M HCl solution, finding that inhibitor efficiency increased with its concentration, reaching a maximum value of 94 % at 500 ppm. According to Langmuir adsorption isotherm, this inhibitor acted as a mixed type of inhibitor and was adsorbed on the steel. Similarly, Carmona-Hernandez *et al.* [13] studied imidazole obtained from palm oil as a corrosion inhibitor for UNS S41425 type supermartensitic stainless steel in an H₂S-containing environment. The authors found that at inhibitor concentrations between 0 and 100 ppm, the maximum inhibitor efficiency was obtained at 25 ppm, decreasing with a further increase of inhibitor concentration. Imidazole was physically adsorbed onto the steel according to Langmuir adsorption isotherm, behaving as a mixed-type of inhibitor. In another work, Abdallah *et al.* [16] evaluated curcumin, parsley and cassia bark extracts as green inhibitors for carbon steel corrosion in 0.5 M sulfuric acid. They found that inhibition efficiency increased with inhibitor concentration, while inhibition efficiency of each particular inhibitor decreased in the following order: cassia bark extract > parsley extract > curcumin extract. Imidazolines obtained from avocado and rice bran oil were obtained and evaluated as CO₂-corrosion inhibitors for X-52 steel [19,20]. Both inhibitors contained fatty acids and were evaluated in concentrations of 0, 5, 10, 25, 50 and 100 ppm. It was found that in both cases, the maximum inhibition efficiency was reached at 25 ppm and decreased with a further increase of inhibitor concentration.

Mamey sapote [*Pouteria sapota*] is a very popular fruit growing in Mexico and Central America [21]. It is a fruit tree that has the potential to be cultivated in 15 of 32 states, *i.e.*, over almost 50 % of the Mexican territory. Its production is concentrated in the south, southeast, west and some central states with an area of 1,618 hectares, with a total production of 20,120 tons of fruit, and a national average yield of 12.4 tons ha⁻¹ [22]. It is a cheap fruit, less than U.S. \$1000 per ton, although currently, oil extraction is somehow expensive. Antioxidant activity of *Pouteria sapota* pulp has already been assessed, finding different phenolic acids, flavonoids, and carotenoids, and the inclusion of such fruit has been recommended in daily diets [23].

Nevertheless, such studies have considered only the flesh and little information exists regarding the seed or bone, although some information suggests the existence of fatty acids [24]. Recently, different researchers evaluated fatty acids contained in palm, avocado and rice bran oil, similar to antioxidants reported for *Pouteria sapota*, as green corrosion inhibitors for steel in CO₂ and H₂S-containing environments [13,19,20]. Thus, the goal of this research is to evaluate use of the oil contained in the *Pouteria sapota* seed to obtain an imidazoline as corrosion inhibitor for 1018 carbon steel in a CO₂-saturated NaCl solution.

Experimental procedure

Materials and sample preparation

The material used in this research work includes bars of 1018 carbon steel having a chemical composition given in Table 1. Specimens were grounded with 1200 grade emerging paper, rinsed with distilled water, acetone and blown with hot air.

Table 1. Chemical composition of 1018 carbon steel

Element	Content, wt.%
Fe	Balance
C	0.14
Mn	0.60
S	<0.05
P	<0.05

Inhibitor synthesis

Imidazoline from *Pouteria sapota* seed oil was obtained by the Soxhlet method to extract the crude oil using hexane as a solvent. Afterward, a bleaching process was carried out on the crude oil using Tonsil and activated carbon in concentrations of 2 and 0.5 %, respectively. This process was performed at 95 °C under constant stirring during 20 min. The oil obtained was filtered under a suction method and mixed with water at 95 °C. Finally, the obtained emulsion was centrifuged to obtain the semi-refined oil. This semi-refined oil was the precursor solution in the synthesis of the imidazoline-based inhibitor. The inhibitor synthesis process was carried out in two stages, as illustrated in Figure 1.

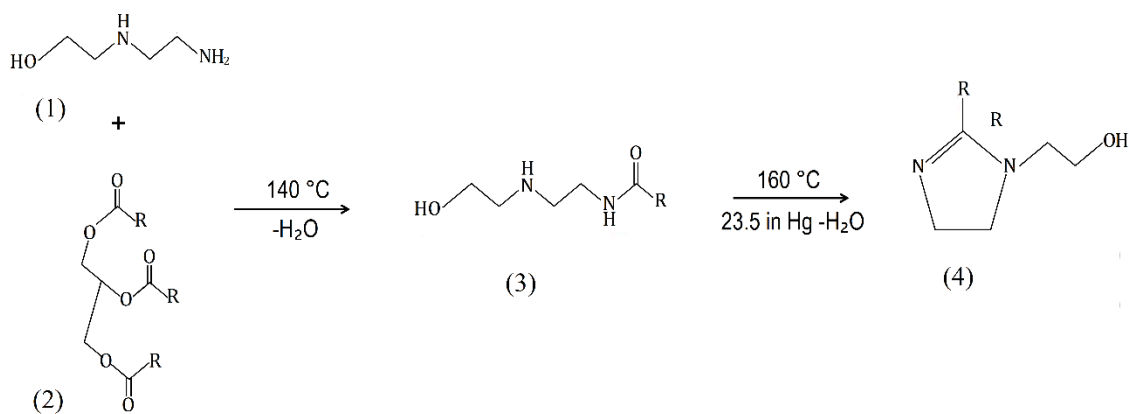


Figure 1. Synthesis of the imidazoline-based inhibitor from semi-refined *Pouteria sapota* oil: (1) *N*-(2-hydroxyethyl) amino ethylamine; (2) *Pouteria sapota* oil; (3) *N*-[2-[(2-hydroxyethyl) amino]ethyl]-amide, fatty amide, and (4) fatty-imidazoline derivative from the raw *Pouteria sapota* oil, where R=alkyl chain of *Pouteria sapota* oil fatty acid

At first, amidation was carried out by hydroxyethyl ethylene diamine during 2.5 hours at 140 °C. This reaction was monitored by the thin layer chromatography technique (TLC) using heptane-ethyl acetate (Sigma Aldrich) (9:1) as eluent. The reaction products were removed by washing and filtering and analysed by the Fourier transform infrared spectroscopy (FTIR) technique. The second synthesis step consisted of performing the imidazoline cyclization reaction. This was carried out once purified fatty-amide was placed at vacuum (79.58 kPa) and heated at 160 °C for 16 hours using (8.5:1.5:5) dichloromethane (Sigma Aldrich), methanol (Baker), ammonium hydroxide (Baker) as eluent while the reaction products were analysed using FTIR. The obtained inhibitor was stored inside a glass beaker

at room temperature. Gas chromatography was used in order to know the type of fatty acids found in the *Pouteria sapota* seed oil as described elsewhere [25]. The oil extracted from *Pouteria sapota* seed was analyzed with an FTIR Spectrophotometer from Bruker. As a corrosive environment, a CO₂-saturated 3.5 % NaCl heated at 50 °C was used according to the NACE standard method NACE TM 177-2005, widely used in the literature [13,19,20,25]. Before starting with corrosion tests, the solution was bubbled with CO₂ gas during 2 hours and the gas bubbling continued during testing. Inhibitor concentrations were chosen to be 0-100 ppm, as were also used in previous works [13,19,20]. These concentrations have also been recommended by manufacturers for commercial imidazolines. Tests were carried out under stagnant conditions as a first inhibitor screening in order to know the optimum inhibitor concentration.

Electrochemical tests

Electrochemical measurements were conducted in a conventional glass cell using a potentiostat from ACM Instruments. Rods of 1018 carbon steel were encapsulated in polymeric resin with an exposed working area of 0.5 cm². As auxiliary and reference electrodes, graphite cylindrical bars and a saturated calomel electrode (SCE) were used. Tests were performed at the temperature of 50 °C. Before starting the experiments, 30 minutes was given for the open circuit potential value (OCP) to reach a steady-state value. Potentiodynamic polarization curves were obtained by applying a cathodic potential 800 mV more negative than the free corrosion potential (E_{corr}) and then the sweeping started in an anodic direction at the scan rate of 1 mV s⁻¹, ending at a potential of 800 mV more anodic than E_{corr} . Tafel extrapolation was used to calculate the corrosion current density values, j_{corr} . Electrochemical impedance spectroscopy (EIS) measurements were performed at the E_{corr} by applying an alternating potential of ± 10 mV in the frequency range between 10 kHz and 0.04 Hz. In order to know the change in the corrosion behavior with time, linear polarization resistance (LPR) measurements were carried out. For this, specimens were polarized ± 15 mV every hour during 24 hours. All experiments were performed three times. The surface of specimens used for LPR experiments was analyzed by the scanning electronic microscope (SEM) LEO VP 1450, whereas chemical analysis of corroded specimens was performed with an X-ray energy dispersive spectrometer (EDS) attached to it.

Results and discussion

Inhibitor characterization

Palmitic acid is the major fatty acid contained in the *Pouteria sapota* oil with 25.5 wt.%, followed by 19.1 % of oleic acid, 16.1 % of myristic acid and 14.1 % of linoleic acid. In Table 2, the full profile of fatty acids contained in the *Pouteria sapota* oil is shown. Chemical structures of palmitic and oleic acids are given in Figure 2.

Table 2. Fatty acid composition of *Pouteria sapota* oil

Fatty acid	Structure	Type of fatty acid	Content of fatty acid, wt. %
Palmitic acid	C16:0	Saturated	24.5
Myristic acid	C14:0	Saturated	16.1
Oleic acid	C18:1 <i>n</i> -9 cis	Unsaturated	19.1
Linoleic acid	C18:2 <i>n</i> -6 cis	Unsaturated	14.1
Linolenic acid	C18:3 <i>n</i> -3 cis	Unsaturated	2.4
Arachidic acid	C20:0	Unsaturated	0.6

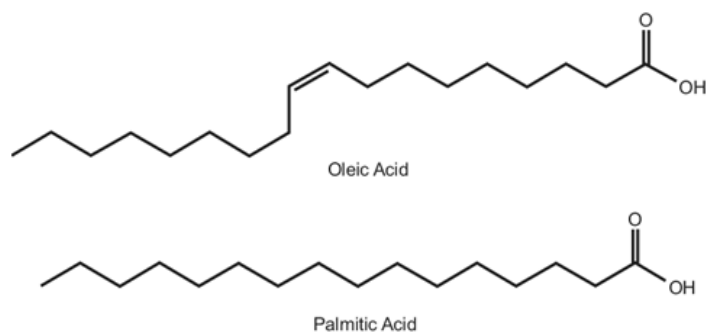


Figure 2. Chemical structures of oleic and palmitic acids

IR spectra of *Pouteria sapota* oil and synthesized inhibitor are shown in Figure 3. The observed C=O stretching signal at 1743 cm^{-1} corresponds to the ester vibration, whereas at 1642 cm^{-1} was assigned to the fatty amide. The inhibitor response presents a signal observed at 1720 cm^{-1} which was assigned to the ester group. Observed peaks at 1560 and 1470 cm^{-1} were assigned to C=C and C=N stretches in the ring of imidazole, whereas another signal observed at 1080 cm^{-1} to C-H stretch. The group N-H of imidazole at 3150 cm^{-1} is due to the aromaticity of the ring. On the other hand, the peak observed at 1630 cm^{-1} corresponds to the C=O stretch of the amide. In addition, observed peaks at 1280 and 1200 cm^{-1} correspond to the stretching of C-N and C-O groups, respectively. Finally, observed signals at 2920 and 2852 cm^{-1} were assigned to the methyl and methylene groups, respectively.

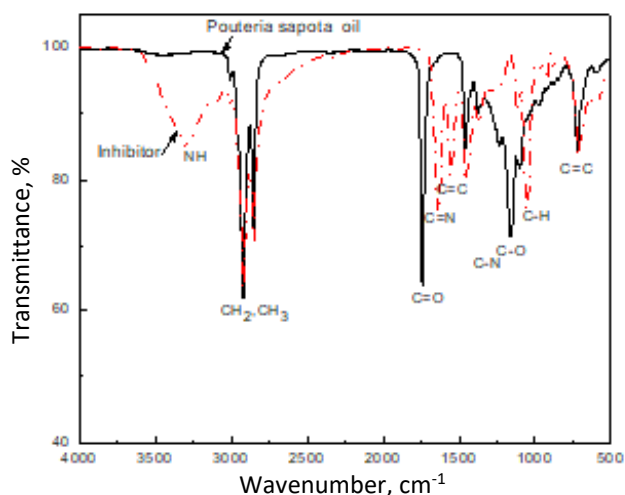


Figure 3. FTIR spectra of *Pouteria sapota* oil and synthesized inhibitor

Open circuit potential

The time changes of OCP values for 1018 carbon steel exposed to the CO_2 -saturated 3.5 % NaCl solution, without and with different inhibitor concentrations, are shown in Figure 4.

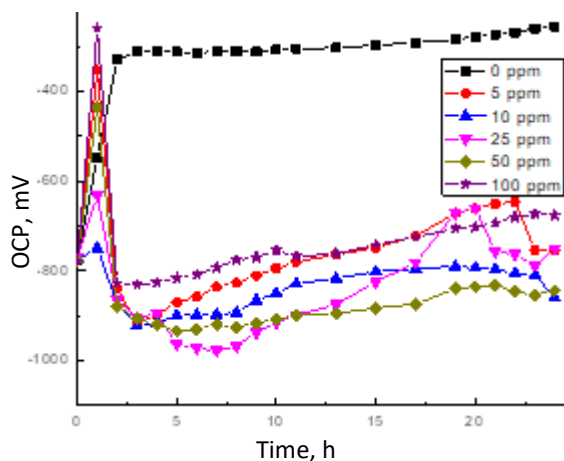


Figure 4. Variation of OCP value with time for 1018 carbon steel in CO_2 -saturated 3.5 % NaCl solution containing different concentrations of inhibitor at 50°C

Figure 4 shows that the OCP value is rapidly shifted towards the noble direction for the blank, uninhibited solution, reaching a steady-state value after 2 or 3 hours of exposure to the environment. This shift can be due to the protection of steel by the formation of iron carbonate film on its surface [26-29]. When the lowest inhibitor concentration (5 ppm) was introduced into the solution, the OCP value became more negative, reaching a steady-state value within 2-3 hours of testing. At higher inhibitor doses, *i.e.*, at 10 and 25 ppm, the OCP value became more negative. With higher doses of inhibitor, however, the OCP value shifted to a noble direction, reaching the noblest value with the addition of 100 ppm. A shift of the OCP value towards more negative values means that the metal is getting corroded, dissolving any protective film formed on the metal surface. On the contrary, if the OCP value moves toward the noble direction, it indicates that the metal has been protected by the formation of a film made from corrosion products [30].

Polarization curves

The effect of inhibitor concentrations on the polarization curve of 1018 carbon steel in the CO₂-saturated 3.5% NaCl solution is shown in Figure 5.

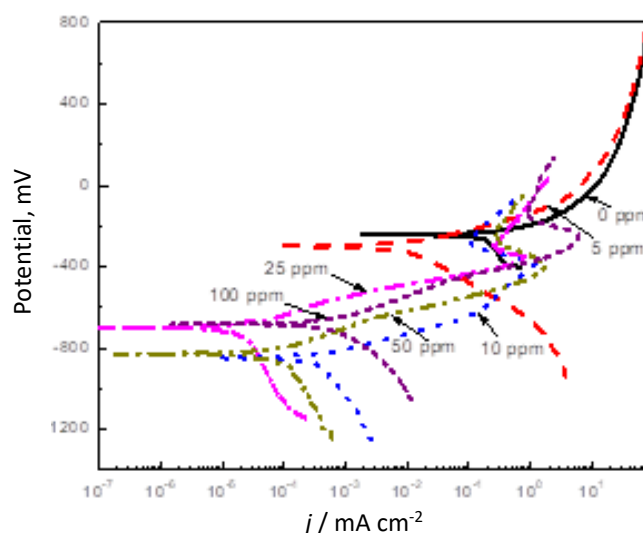


Figure 5. Effect of inhibitor concentrations on polarization curve of 1018 carbon steel in CO₂-saturated 3.5 % NaCl solution at 50°C

Figure 5 shows that in the uninhibited solution, there is no evidence of the existence of any passive layer on the steel surface. Similar behavior is observed when 5 ppm of inhibitor were added into the system, although j_{corr} value decreased from a value of 2.0×10^{-1} mA/cm² down to 10^{-2} mA/cm² as shown in Table 3. In the absence of inhibitor and in the CO₂ environment, iron carbonate film, which is not protective, is developed on the steel surface, which is why the passive layer was not formed. With the addition of low doses of inhibitor, inhibitor reacts with the released iron ions, forming a layer of corrosion products that acts as a barrier between the metal and the environment. This barrier makes their contact more difficult, which results in a decrease of j_{corr} value. As the inhibitor doses increased up to 25 ppm, a significant reduction in the j_{corr} value can be observed, reaching its lowest value of 3.0×10^{-5} mA/cm². After a further increase of the inhibitor concentration, however, j_{corr} increased again. Generally, a decrease of j_{corr} value with the addition of inhibitor is due to its adsorption on the steel surface and the formation of a passive layer. As the inhibitor concentration increases, the number of its molecules covering the steel surface increases too, and due to the existence of the same electric charge, there is an electrostatic repulsion among

inhibitor molecules. This results in the inhibitor desorption from the steel surface, leaving the unprotected metal at the places of desorption. Salinas-Solano *et al.* [19] reported the lowest j_{corr} value of 2.34×10^{-4} mA/cm² whereas Cruz-Zabalegui *et al.* [20] reported the value of 6.0×10^{-3} mA/cm² for carbon steel in CO₂-saturated 3.5 % NaCl solution, by using amino surfactants and imidazolines obtained from avocado and rice bran oil, respectively. Both reported j_{corr} values are, however, much higher than the minimal value of $j_{\text{corr}} = 3.0 \times 10^{-5}$ mA/cm² reported in this study (Table 3). Polarization curves for inhibitor concentrations higher than 5 ppm in Figure 5 displayed the presence of a passive layer.

The values of j_{corr} were used to calculate the inhibitor efficiency values (*IE*) as follows:

$$IE = \frac{j_{\text{corr}} - j_{\text{corr/inh}}}{j_{\text{corr}}} 100 \quad (1)$$

where the corrosion current density values obtained in the absence and presence of the inhibitor are represented by j_{corr} and $j_{\text{corr/inh}}$, respectively. Calculated *IE* values are listed in Table 3.

Table 3. Electrochemical parameters obtained from polarization curves

$C_{\text{inh}} / \text{ppm}$	$E_{\text{corr}} / \text{mV}$	$j_{\text{corr}} / \text{mA cm}^{-2}$	$E_{\text{pit}} / \text{mV}$	$\beta_a / \text{mV dec}^{-1}$	$\beta_c / \text{mV dec}^{-1}$	<i>IE</i> / %	θ
0	-240	2.0×10^{-1}	-	50	245		
5	-300	3.0×10^{-2}	-	60	200	95.0	0.95
10	-850	3.0×10^{-4}	-255	65	380	99.8	0.99
25	-700	3.0×10^{-5}	-290	70	400	99.9	0.99
50	-830	2.0×10^{-5}	-230	75	450	99.9	0.99
100	-680	6.0×10^{-4}	-110	80	300	99.7	0.99

Data in Table 3 show an increase in the inhibitor efficiency value with an increase in its concentration up to 25 ppm, and a decrease for higher concentrations. The fractional surface coverage by the inhibitor (θ), which was calculated by dividing the inhibitor efficiency value by 100, behaves in the same fashion as the inhibitor efficiency. The highest efficiency value of 99 % was obtained with the addition of 25 ppm, which is similar to the reported by Salinas-Solano *et al.* [19] but higher than 93 % reported by Cruz-Zabalegui *et al.* [20]. Zheng *et al.* [31] used a mercaptopropionic acid-modified oleic imidazoline as a highly efficient corrosion inhibitor for carbon steel in CO₂-saturated formation water and obtained *IE* value of 95 % with the addition of 20 ppm. At the same time, j_{corr} value was decreased for 2 orders of magnitude. Sotelo-Mazon *et al.* [32] obtained *IE* of 99 % with-imidazoline synthesized from wasted avocado oil for carbon steel in CO₂-saturated 3.5 % NaCl solution, and j_{corr} value was reduced for 2 orders of magnitude, from 0.1 to 0.001 mA cm⁻². Okafor *et al.* [33] obtained an inhibitor efficiency of 97 % with the addition of 200 ppm of a rosin amide imidazoline for N80 carbon steel in CO₂-saturated simulated formation water, with the reduction of j_{corr} value from 0.1 down to 0.005 mA cm⁻². Therefore, the present results, which show that for a relatively low inhibitor concentration of 25 ppm, high inhibitor efficiency of 99 % is attained and j_{corr} value is reduced for even four orders of magnitude, are very encouraging. All these justify the use of *Pouteria sapota*, not only because it is a green inhibitor but also because it is obtained from a waste agro-industrial product that is a very abundant product in our country that can be utilized in this way.

A possible effect of pitting corrosion, which is a localized type of corrosion characteristic for breaking of passive film on stainless steel in solutions containing chloride ions, is further explored. The effect of the inhibitor concentration on the pitting potential (E_{pit}) value can be seen in Table 2. Since no passive film formation at 0 and 5 ppm was observed, there is no value for E_{pit} at these inhibitor concentrations. However, it can be seen that at the inhibitor concentration of 10 ppm, E_{pit}

value of -255 mV is observed, and it became more active at 25 ppm, showing E_{pit} of -290 V. As the inhibitor concentration increased further, E_{pit} attained more positive values of -230 and -110 mV at inhibitor concentrations of 50 and 100 ppm, respectively.

Data in Table 2 clearly shows that anodic Tafel slopes remained virtually unaffected by the addition of the inhibitor, unlike the cathodic one, which was greatly affected, indicating that this inhibitor behaves as a mixed-type of inhibitor with a predominant cathodic effect. This way, it can be said that anodic reactions such as iron dissolution remained practically unaffected by the addition of the inhibitor, whereas cathodic reactions such as oxygen reduction and hydrogen evolution (HE) were severely affected. This indicates that this inhibitor blocked the sites where protons can be adsorbed on the metal surface for the HE reaction [34,35].

It has already been established that the adsorption of an organic compound such as an inhibitor on a metal surface depends, among other things, upon its chemical structure and chemical compositions of substrate and electrolyte [36]. At the steel/electrolyte interface, an organic compound can be absorbed by: i) electrostatic interaction between metal and inhibitor, ii) interaction between the inhibitor uncharged electron pairs and metal surface, and iii) interaction of π electrons of inhibitor with the metal [25]. In order to get more information about the way of interaction between an inhibitor and metal, it is necessary to know the adsorption isotherm. In Figure 6, different adsorption isotherm models, *i.e.*, Langmuir, Temkin and Frumkin, are tested with data obtained for different concentrations of Pouteria sapota oil as an inhibitor for 1018 carbon steel in CO₂ saturated 3.5 % NaCl.

It is obvious from Figure 6 that the best fit to predicted linear dependences, measured by the correlation factor (R^2), were obtained for the Langmuir type of adsorption isotherm. For this isotherm, this factor was 0.99, whereas, for Temkin and Frumkin isotherms, it had values of 0.70 and 0.79, respectively. This factor is a measure of the correlation between experimental and predicted data, and closer to the unit, the better is the correlation.

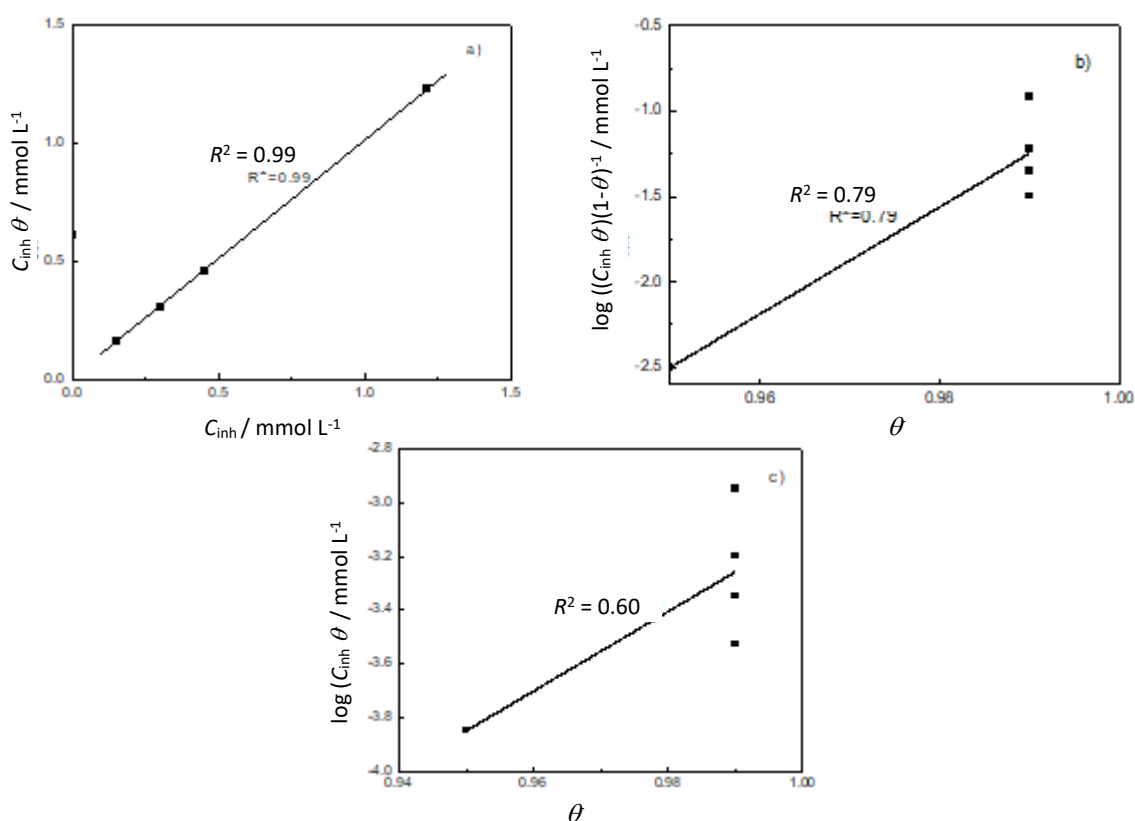


Figure 6. a) Langmuir, b) Frumkin and c) Temkin isotherm plots for 1018 carbon steel in CO₂-saturated 3.5% NaCl solution containing different concentrations of inhibitor at 50 °C

Langmuir isotherm assumes that the interaction between molecules and a surface can be described by a simple equilibrium, with the equilibrium constant K_{ads} . It does not take the interaction between adsorbed molecules into account, nor modification of the surface by the adsorption. Langmuir adsorption isotherm is a function between the fractional surface coverage by the inhibitor (θ) and its concentration (C_{inh}) according to equation (2):

$$\frac{C_{\text{inh}}}{\theta} = \frac{1}{K_{\text{ads}}} + C_{\text{inh}} \quad (2)$$

The adsorption equilibrium constant K_{ads} has a relationship with the standard free energy of adsorption (ΔG^0_{ads}) through the following equation (3):

$$G^0_{\text{ads}} = -RT \ln(10^6 K_{\text{ads}}) \quad (3)$$

where R is the universal gas constant, and T is the absolute temperature. Using data from Figure 6a, the calculated value for ΔG^0_{ads} was $-43.34 \text{ kJ mol}^{-1}$, indicating strong adsorption on the metal surface due to the sharing of charges between the molecules and/or the formation of coordinated type bonds (chemisorption).

One of the explanations for the high inhibitory effect of imidazoline is the presence of nitrogen atoms located in the structural ring, as well as the high number of carbon atoms in the molecule, which will act as a barrier against electrolyte. Also, double bonds in the compound chemical structure have been reported as part of this high inhibitory efficiency [36]. Compounds found by the gas chromatography analysis detected the presence of palmitic (C16:0), myristic (C14:0), oleic (C18:1 *n*-9 *cis*), linoleic (C18:2 *n*-6 *cis*) and linolenic (C18:3 *n*-3 *cis*) acids in proportions of 24.5, 16.1, 19.1, 14.1 and 2.4 wt.% [36]. These compounds meet two characteristics that make an organic compound a very efficient inhibitor, i.e., long chains of hydrocarbons and the presence of double bonds.

Linear polarization resistance (LPR) measurements

Data given in Figure 7 represent the variation on the polarization resistance (R_p) value with the inhibitor concentration in the CO_2 environment.

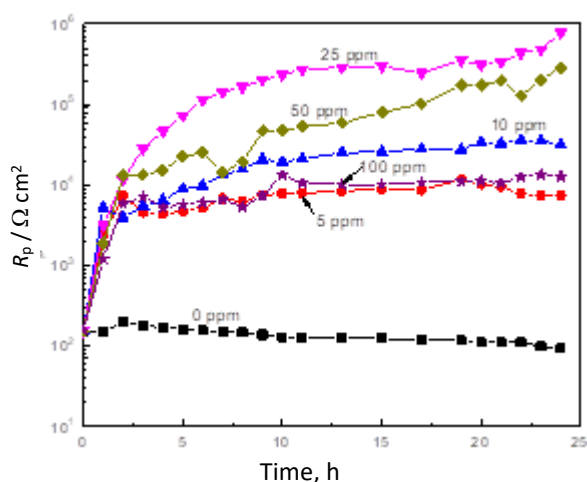


Figure 7. Effect of inhibitor concentration on R_p value for 1018 carbon steel in CO_2 -saturated 3.5 % NaCl solution containing different concentrations of inhibitor at 50 °C

For uninhibited solution, R_p value remained practically constant throughout the testing time, exhibiting a relatively low value, close to $100 \Omega \text{ cm}^2$. A remarkable increase of R_p value was observed as soon as the inhibitor was added into the solution, which is believed to be due to the adsorption of the inhibitor onto the steel surface. As long as the metal surface area covered by the inhibitor increases, the value for R_p increases too. In the same way, as the inhibitor concentration increases, an increase of R_p value was also observed, but only up to the inhibitor concentration of 25 ppm. The

obtained R_p values were up to four orders of magnitude higher than that obtained in the uninhibited solution. With a further increase of the inhibitor concentration, R_p values decreased, which can be due to the electrostatic repulsion between inhibitor molecules, when they are too many and very close to each other that a desorption process occurs.

It was already shown [36] that the tested inhibitor is not a pure compound because it contains fatty acids (Table 2), where the main are oleic and palmitic acids with chemical structures given in Fig. 3, although the presence of myristic and linoleic acids is important also. It is not very clear which one of these compounds is responsible for corrosion inhibition, but it is very likely that it is due to a synergistic effect of different compounds. The presence of N atoms in the imidazole group makes these fatty acids highly susceptible to protonation [37]. However, as established above, organic compound structure affects its performance, and according to Jovancicevic *et al.* [38], it was found that the longer the alkyl group's hydrocarbons chain is, the compound is a more efficient inhibitor. Alternatively, the presence of double bonds into the inhibitor structure improved the inhibitor adsorption onto the steel surface [38]. Thus, the presence of compounds with long hydrophobic chains and double bonds, in addition to the presence of N atoms susceptible to protonation, makes this inhibitor highly efficient.

EIS measurements

In order to elucidate the corrosion mechanism for 1018 carbon steel in CO₂-saturated 3.5 % NaCl solution in the absence and presence of inhibitor, some EIS measurements at the open circuit potential were performed. Figure 8 shows the results presented in both Nyquist and Bode formats.

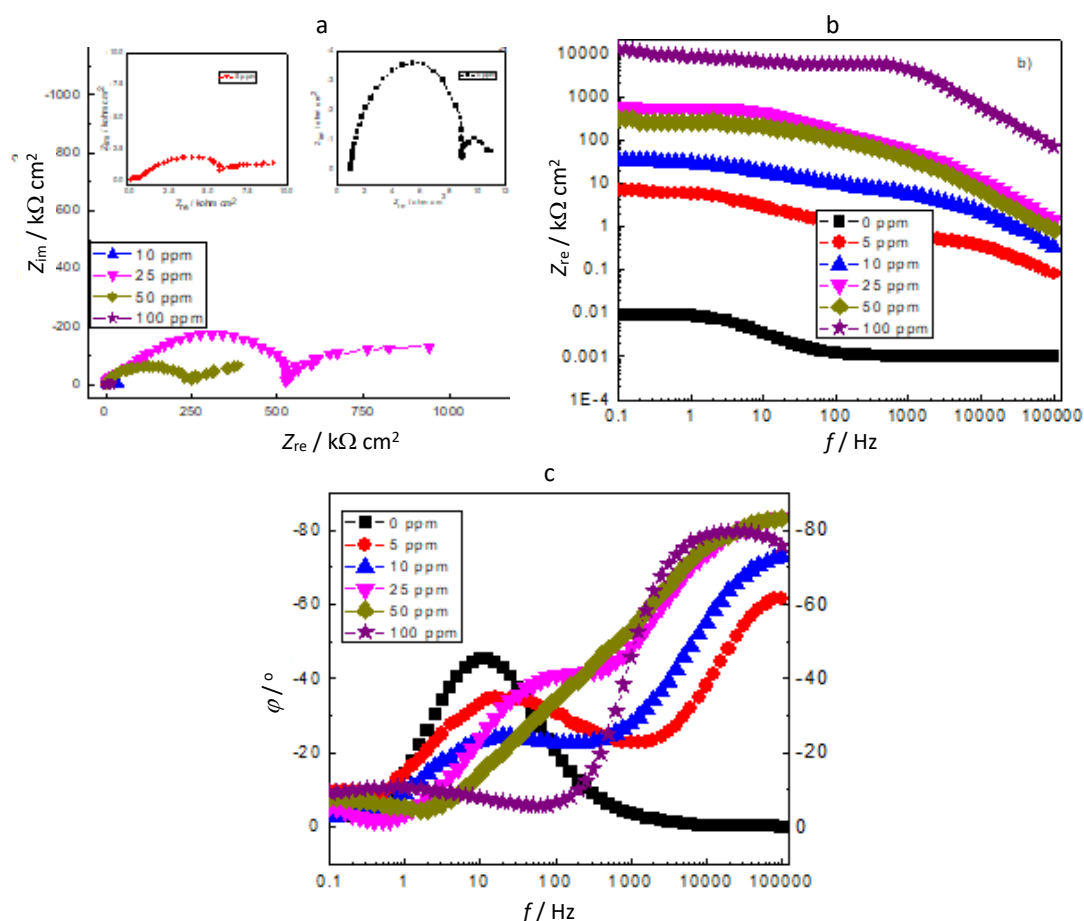


Figure 8. Effect of inhibitor concentration on: a) Nyquist and b) and c) Bode plots of 1018 carbon steel in CO₂-saturated 3.5 % NaCl solution containing different concentrations of inhibitor at 50 °C

Nyquist data display two capacitive semicircles, one at high to medium frequencies and the other at the lowest frequencies (Figure 8a). The resulting semicircles seem to be imperfect due to the heterogeneity and roughness of the sample surface. The first, high-frequency semicircle, is related to the formation of corrosion products, whereas the second, lower frequency semicircle, is related to the electrochemical double-layer and charge transfer reaction due to corrosion. The shapes of Nyquist and Bode plots did not change with the addition of inhibitor, indicating that the corrosion mechanism is not affected by inhibitor addition. The semicircle diameters, however, increased with an increase of inhibitor concentration, reaching the highest values at 25 ppm of inhibitor. A further increase of the inhibitor concentration above 25 ppm caused a decrease of semicircle diameters.

On the other hand, Bode plots in the modulus format (Figure 8b) showed that at the lowest frequencies, impedance modulus is the lowest for the solution in the absence of an inhibitor. Impedance modulus increased with the inhibitor concentration, attaining more than four orders higher magnitude with the addition of 25 ppm of inhibitor. A further increase in the inhibitor concentration caused a decrease in the low-frequency impedance modulus value. The modulus impedance value at the lowest frequency takes into account all resistance contributions such as electrolyte or solution resistance (R_s), charge transfer resistance through double electrochemical layer (R_{ct}) and the resistance of the film formed by the corrosion products (R_f). Since the sum of the last two, *i.e.*, $R_{ct} + R_f$ is defined as the polarization resistance value (R_p), we can see that the variation of the lowest frequency impedance modulus value observed in Figure 8b behaves in the same way as R_p in Figure 7.

At higher frequencies, impedance modulus data in Figure 8b show sloping lines characteristic of capacitive impedance responses, where higher impedance values imply lower capacitance values. It is seen in Figure 8b that capacitive impedances increased (capacitance decreased) with the addition of inhibitor up to 25 ppm, and decreased (capacitance increased) for higher inhibitor concentrations. It has already been known that two different electric interface values, such as electrical resistance and capacitance, are inversely proportional [37-43], and thus, an increase in the resistance value decreases the capacitance value. This proves the ability of the studied extract to reduce the aggressive action of the acid medium. According to the Helmholtz model, the reduction in the capacitance value indicates an increase of the double layer thickness, which can be referred to as the development of a compact protective film on the metal surface by the inhibitor adsorption [44-46].

The phase angle Bode plots (Figure 8c) show the presence of two peaks, one at higher and the other at lower frequencies, defining two separate relaxations (RC) time constants characteristic for interfacial and film regions. These suggest two phenomena are happening and that the corrosion process is not only under interfacial charge transfer control.

Surface analysis

SEM micrographs of corroded steel surfaces in CO₂-saturated 3.5 % NaCl solution in the absence and presence of inhibitor are shown in Figure 9. For corroded steel surface in the absence of inhibitor, Figure 9a presents a high area that corroded uniformly, just as predicted by polarization and R_p results.

Similar is observed in Figure 9b, presenting the image of steel surface when 5 ppm of inhibitor were added to the solution, although the corroded surface area is somewhat smaller in the presence of the inhibitor. As the amount of inhibitor was increased further, the corrosion type shifted from uniform to a localized type of corrosion such as pitting corrosion, which is clearly seen in Figure 9c. The surface with the lowest damaged area by corrosion was found for steel corroded in the presence of 25 ppm of inhibitor, shown in Figure 9d. Here, the number of pits is the lowest, as predicted by polarization curves and R_p measurements shown in Figures 3 and 6, respectively.

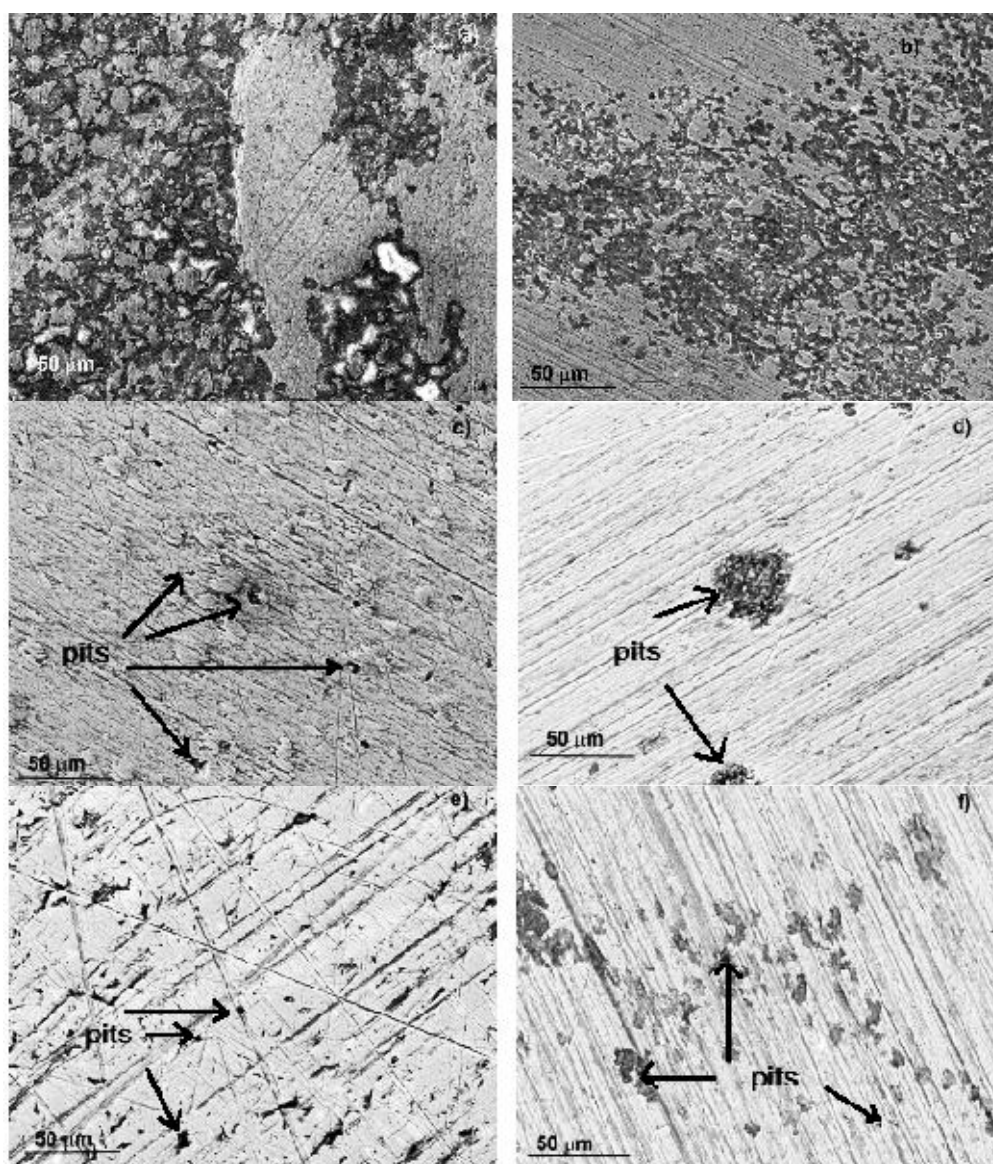


Figure 9. SEM micrographs of 1018 carbon steel corroded in CO₂-saturated 3.5% NaCl solution at 50 °C containing following concentrations of inhibitor: a) 0; b) 5; c) 10; d) 25; e) 50; f) 100 ppm

EDS microchemical analysis performed on the corrosion products layer is presented in Figure 10. For specimens corroded in the absence of inhibitor, Figure 10a shows only chemical elements present in the steel and the corrosive environment such as Fe, C and O. For specimens corroded in the presence of the inhibitor (Figure 10b-d), Fe, C and O were also present, but the amounts of C and O were higher than found in specimens corroded in the absence of inhibitor since imidazoline contains both chemical elements. Elements present in the abrasives, such as Al from Al₂O₃ particles and SiC in the abrading paper, were also present.

Thus, the addition of the inhibitor decreased not only the corrosion rate but also the type of corrosion, changing it from the uniform type in the absence of inhibitor to a localized type of corrosion when the inhibitor is added. This is expected since for inhibitor concentrations higher than 5 ppm a passive layer is formed on the top of the steel according to polarization curves shown in Figure 5, and this passive layer can be disrupted, giving place to localized type of corrosion such as pitting.

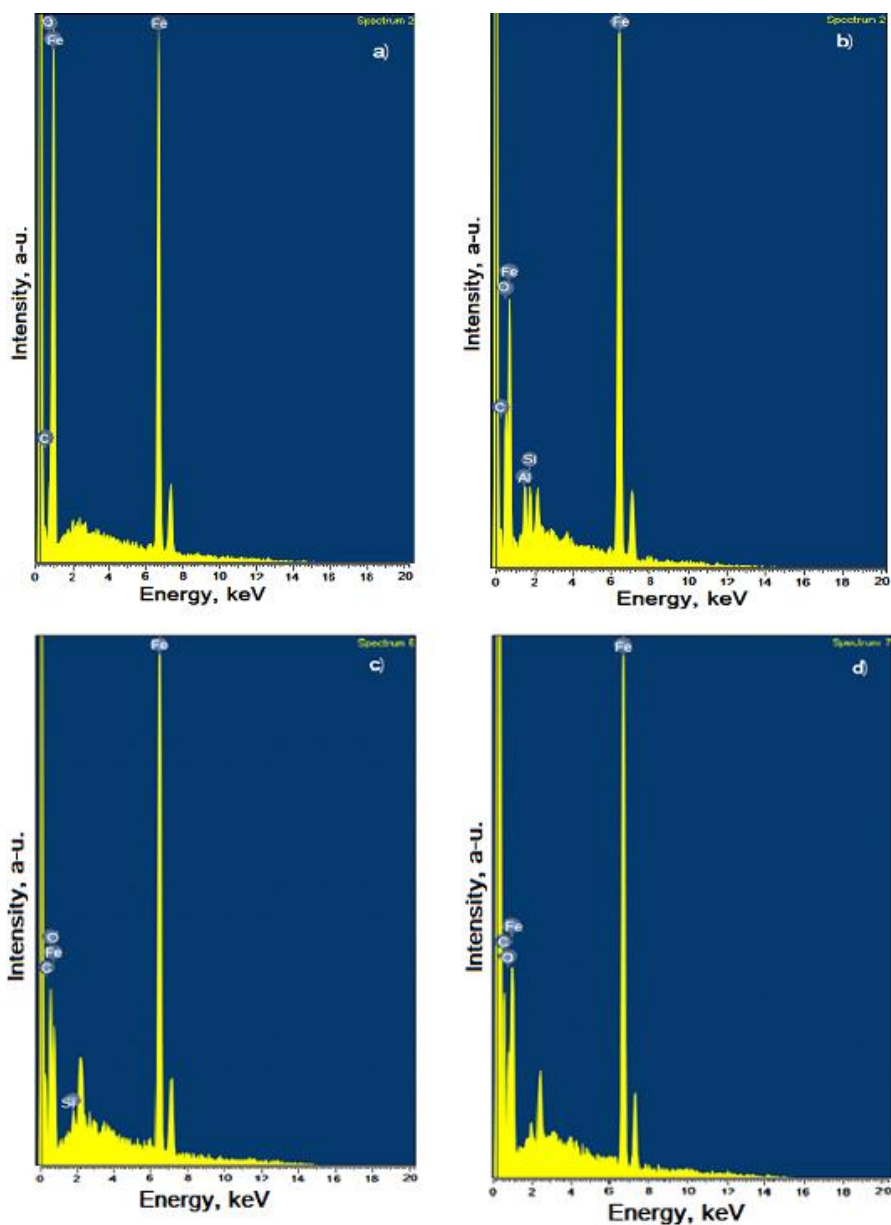


Figure 10. EDS microchemical analysis of corrosion products layer formed on 1018 carbon steel corroded in CO_2 -saturated 3.5% NaCl solution at 50 °C, containing following concentrations of inhibitor: a) 0; b) 5; c) 10; d) 25 ppm

Corrosion inhibition mechanism

As mentioned above, the obtained imidazoline is chemically adsorbed on the steel surface due to the sharing of charges between molecules and/or the formation of coordinated type bonds. Imidazoline contains a hydrophilic, imidazole group, and a hydrophobic alkyl group given by fatty acids, which present saturated and unsaturated structures. The high inhibitory effect of imidazoline compounds has been related to the structure of the inhibitor due to the nitrogen atoms located in the structural ring, to the long chain of hydrocarbons acting as a barrier against water and chlorides, and finally, to unsaturated double bonds present in the inhibitor which is chemically adsorbed on the surface of Fe (which form a very stable protective film). To give a better explanation about the corrosion inhibition process in the presence of the antioxidant constituents of the extract on the steel surface, a schematic diagram of the adsorption is shown in Figure 11.

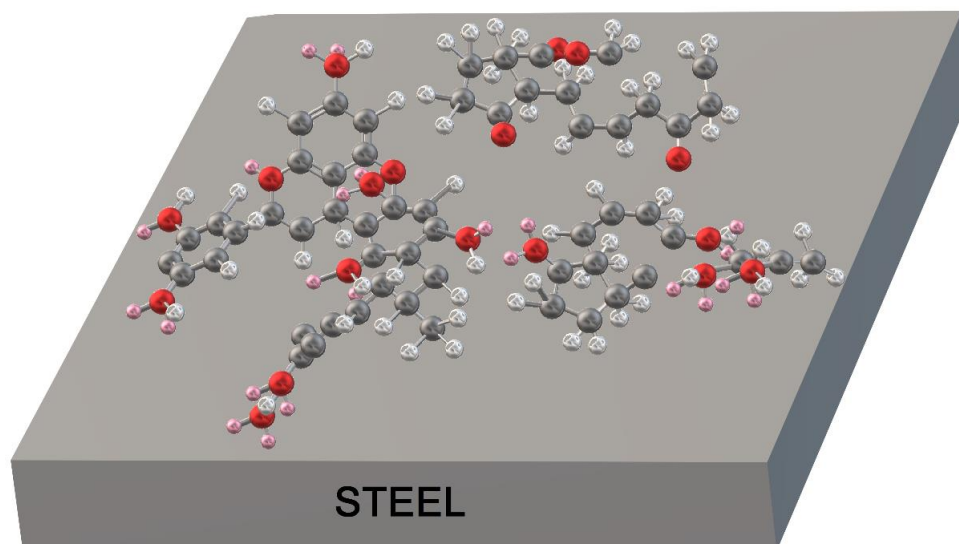


Figure 11. Chemisorption process between antioxidant constituents in *Pouteria sapota* extract. Unshared pairs of electrons are in pink color, heteroatoms in red, and π bond orbitals are the dotted line

Compounds contained in the *Pouteria sapota* extract have a strong electron-donating and chelating capacity with steel, giving the extract the ability to inhibit metal corrosion. This chemisorption is preferable by an electronic interaction between unshared pairs of electrons from heteroatoms and π bond orbitals from the molecules and the benzene rings with the d orbitals on the metallic surface until the formation of a very adherent barrier of molecules.

Conclusions

An imidazoline obtained from fatty acids contained in *Pouteria sapota* seed oil has been evaluated as an inhibitor for CO₂ corrosion of 1018 carbon steel in 3.5 % NaCl at 50 °C. It was found that the main fatty acids are palmitic, oleic, myristic and linoleic acid. The obtained imidazoline was proved to be an excellent mixed-type of inhibitor, which affected both cathodic and anodic reactions but with a stronger effect on the cathodic one. The inhibitor is chemically adsorbed onto the steel surface according to the Langmuir type of adsorption isotherm. Inhibitor efficiency increased with its concentration up to 25 ppm, but after this critical concentration, its efficiency decreased. Polarization curves indicated that I_{corr} value decreased more than four orders of magnitude when 25 ppm of inhibitor were added due to the formation of a passive layer onto the steel surface. This is supported by EIS data that showed two separate relaxation processes due to interfacial and film regions. The type of corrosion was affected by the addition of inhibitor, changing from the uniform to a localized type of corrosion.

References

- [1] T. Pojtanabuntoeng, M. Salasi, *Electrochimica Acta* **258** (2017) 442-452. <https://doi.org/10.1016/j.electacta.2017.11.081>
- [2] T. Doi, T. Adachi, T. Kudo, N. Usuki, *Corrosion Science* **117** (2020) 108931. <https://doi.org/10.1016/j.corsci.2020.108931>
- [3] F. E. Abeng, V. Anadebe, P. Y. Nkom, K. J. Uwakwe, E. G. Kamalu, *Journal of Electrochemical Science and Engineering* **11**(1) (2021) 11-26. <https://doi.org/10.5599/jese.887>
- [4] W. Boukhedena, S. Deghboudj, *Journal of Electrochemical Science and Engineering* **11**(4) (2021) 227-239. <https://doi.org/10.5599/jese.1050>
- [5] S. Bashir, V. Sharma, H. Lgaz, I. M. Chung, A. Singh, A. Kumar, *Journal of Molecular Liquids* **263** (2018) 454-462. <https://doi.org/10.1016/j.molliq.2018.04.143>

- [6] R. T. Loto, C. A. Loto, *Journal of Materials Research and Technology* **7**(3) (2018) 231-239. <https://doi.org/10.1016/j.imrt.2017.07.004>
- [7] A. Kahyarian, A. Schumaker, B. Brown, S. Nestic, *Electrochimica Acta* **258** (2017) 639-652. <https://doi.org/10.1016/j.electacta.2017.11.109>
- [8] M. Chellouli, D. Chebabe, A. Dermaj, H. Erramli, N. Bettach, N. Hajjaji, M. P. Casaletto, C. Cirrincione, A. Privitera, A. Srhiri, *Electrochimica Acta* **204** (2016) 50-59. <https://doi.org/10.1016/j.electacta.2016.04.015>
- [9] L. Pezzato, M. Lago, K. Brunelli, M. Breda, I. Calliari, *Journal of Materials Engineering and Performance* **27**(8) (2018) 3859-3668. <https://doi.org/10.1007/s11665-018-3408-5>
- [10] X. Liu, J. Jing, Q. Fu, Q. Li, S. Li, Y. Qu, A. Singh, *International Journal of Electrochemical Science* **14**(6) (2019) 8819-8835. <https://doi.org/10.20964/2019.09.26>
- [11] G. T. Galo, A. de A. Morandim-Gianneti, F. Cotting, I. V. Aoki, I. Pacifico Aquino, *Metals and Materials International* **27**(10) (2021) 3238-3249. <https://doi.org/10.1007/s12540-020-00679-9>
- [12] M. Abdallah, H. M. Altass, A. S. Al-Gorair, J. H. Al-Fahemi, B. A. A. L. Jahdaly, K. A. Soliman, *Journal of Molecular Liquids* **323** (2021) 115036. <https://doi.org/10.1016/j.molliq.2020.115036>
- [13] A. Carmona-Hernandez, E. Vazquez-Velez, J. Uruchurtu-Chavarin, J. G. Gonzalez-Rodriguez, L. Martinez-Gomez, *Green Chemistry Letters and Reviews* **12**(1) (2019) 89-99. <https://doi.org/10.1080/17518253.2019.1578997>
- [14] M. Abdallah, A. Al Bahir, H. M. Altass, A. Fawzy, N. El Guesmi, A. S. Al-Gorai, F. Benhiba, I. Warad, A. Zarrouk, *Journal of Molecular Liquids* **330** (2021) 115702. <https://doi.org/10.1016/j.molliq.2021.115702>
- [15] A. Chraka, I. Raissouni, N. B. Seddik, *Journal of Bio- and Tribo-Corrosion* **6**(1) (2020) 80. <https://doi.org/10.1007/s40735-020-00377-4>
- [16] M. Abdallah, H. M. Altass, B. A. AL Jahdaly, M. M. Salem, *Green Chemistry Letters and Reviews* **11**(3) (2018) 189-196. <https://doi.org/10.1080/17518253.2018.1458161>
- [17] M. Abdallah, K. A. Soliman, A. S. Al-Gorair, A. Al Bahir, J. H. Al-Fahemi, M. S. Motawea, S. S. Al-Juaid, *RSC Advances* **11**(28) (2021) 17092-17107. <https://doi.org/10.1039/D1RA01010G>
- [18] A. H. Al-Bagawi, *Green Chemistry Letters and Reviews* **14**(1) (2021) 73-84. <https://doi.org/10.1080/17518253.2020.1862923>
- [19] G. Salinas-Solano, J. Porcayo-Caldero, L. M. Martinez de la Escalera, J. Canto, M. Casales-Diaz, O. Sotelo-Mazon, J. Henao, L. Martinez-Gomez, *Industrial Crops and Products* **119** (2018) 111-124. <https://doi.org/10.1016/j.indcrop.2018.04.009>
- [20] A. Cruz-Zabalegui, E. Vazquez-Velez, G. Galicia-Aguilar, M. Casales-Diaz, R. Lopez-Sesenes, J. G. Gonzalez-Rodriguez, L. Martinez-Gomez, *Industrial Crops and Products* **133** (2019) 203-211. <https://doi.org/10.1016/j.indcrop.2019.03.011>
- [21] R. M. Martínez-Casares, H. Pérez, N. Manjarrez, M. Solís-Oba, L. Ortega, A. Solís, *Industrial Crops and Products* **153** (2020) 112606. <https://doi.org/10.1016/j.indcrop.2020.112606>
- [22] J. Martínez-Castillo, N. H. Blancarte-Jasso, G. Chepe-Cruz, N. G. Nah-Chan, M. M. Ortiz-García, *Tree Genetics & Genomes* **15** (2019) 61-68. <https://doi.org/10.1007/s11295-019-1368-z>
- [23] E. Murillo, A. Agócs, V. Nagy, S. B. Király, T. Kurtán, E. M. Toribio, J. Lakey-Beitia, J. Deli, *Chirality* **32**(5) (2020) 579-587. <https://doi.org/10.1002/chir.23206>
- [24] E. Reyes-Dorantes, J. Zuñiga-Díaz, A. Quinto-Hernandez, J. Porcayo-Calderon, J. G. Gonzalez-Rodriguez, L. Martinez-Gomez, *Journal of Chemistry* **2017** (2017) 2871034. <https://doi.org/10.1155/2017/2871034>
- [25] L. Zeng, G. A. Zhang, X. P. Guo, C.W. Chai, *Corrosion Science* **90** (2015) 202-215. <https://doi.org/10.1016/j.corsci.2014.10.011>

- [26] H. Liu, T. Gu, G. Zhang, H. Liu, Y. F. Cheng, *Corrosion Science* **136** (2018) 47-59. <https://doi.org/10.1016/j.corsci.2018.02.038>
- [27] Z. Liu, X. Gao, L. Du, J. Li, P. Li, C. Yu, R. D. K. Misra, Y. Wang, *Electrochimica Acta* **232** (2017) 528-541. <https://doi.org/10.1016/j.electacta.2017.02.114>
- [28] D. Burkle, R. De Motte, W. Taleb, A. Kleppe, T. Comyn, S.M. Vargas, A. Neville, R. Barker, *Electrochimica Acta* **255** (2017) 127-144. <https://doi.org/10.1016/j.electacta.2017.09.138>
- [29] K. Rahmouni, M. Keddami, A. Srhiri, H. Takenouti, *Corrosion Science* **47(12)** (2005) 3249-3266. <https://doi.org/10.1016/j.corsci.2005.06.017>
- [30] M. Vemula, A. S. Shaikh, S. Chilakala, M. Tallapally, V. Upadhyayula, *Food Additives and Contaminants A* **37(10)** (2020) 1601-1609. <https://doi.org/10.1080/19440049.2020.1794055>
- [31] Z. Zheng, J. Hu, N. Eliaz, L. Zhou, X. Yuan, X. Zhong, *Corrosion Science* **194** (2021) 109930. <https://doi.org/10.1016/j.corsci.2021.109930>
- [32] O. Sotelo-Mazon, S. Valdez, J. Porcayo-Calderon, M. Casales-Diaz, J. Henao, G. Salinas-Solano, J. L. Valenzuela-Lagarda, L. Martinez-Gomez, *Green Chemistry Letters and Reviews* **12(3)** (2019) 255-270. <https://doi.org/10.1080/17518253.2019.1629698>
- [33] P. C. Okafor, C. B. Liu, Y. J. Zhu, Y. G. Zheng, *Industrial Engineering and Chemical Research* **50(12)** (2011) 7273-7281. <https://doi.org/10.1021/ie1024112>
- [34] S. A. Pauline, S. Sahila, C. Gopalakrishnan, S. Nanjundan, N. Rajendran, *Progress in Organic Coatings* **72(3)** (2011) 443-452. <https://doi.org/10.1016/j.porgcoat.2011.06.001>
- [35] Z. Liu, X. Gao, L. Du, J. Li, P. Li, C. Yu, R. D. K. Misra, Y. Wang, *Electrochimica Acta* **232** (2017) 528-541. <https://doi.org/10.1016/j.electacta.2017.02.114>
- [36] D. Burkle, R. De Motte, W. Taleb, A. Kleppe, T. Comyn, S. M. Vargas, A. Neville, R. Barker, *Electrochimica Acta* **255** (2017) 127-144. <https://doi.org/10.1016/j.electacta.2017.09.138>
- [37] K. Rahmouni, M. Keddami, A. Srhiri, H. Takenouti, *Corrosion Science* **47(12)** (2005) 3249-3266. <https://doi.org/10.1016/j.corsci.2005.06.017>
- [38] V. Jovancicevic, S. Ramachandran, P. Prince, *Corrosion* **55(5)** (1999) 449-456. <https://doi.org/10.5006/1.3284006>
- [39] M. Vemula, A. S. Shaikh, S. Chilakala, M. Tallapally, V. Upadhyayula, *Food Additives and Contaminants: Part A* **37(10)** (2020) 1601-1609. <https://doi.org/10.1080/19440049.2020.1794055>
- [40] Z. Zheng, J. Hu, N. Eliaz, L. Zhou, X. Yuan, X. Zhong, *Corrosion Science* **194** (2022) 109930. <https://doi.org/10.1016/j.corsci.2021.109930>
- [41] O. Sotelo-Mazon, S. Valdez, J. Porcayo-Calderon, M. Casales-Diaz, J. Henao, G. Salinas-Solano, J. L. Valenzuela-Lagarda, L. Martinez-Gomez, *Green Chemistry Letters and Reviews* **12(3)** (2019) 255-270. <https://doi.org/10.1080/17518253.2019.1629698>
- [42] P. C. Okafor, C. B. Liu, Y. J. Zhu, Y. G. Zheng, *Industrial & Engineering Chemistry Research* **50(12)** (2011) 7273-7281. <https://doi.org/10.1021/ie1024112>
- [43] S. A. Pauline, S. Sahila, C. Gopalakrishnan, S. Nanjundan, N. Rajendran, *Progress in Organic Coatings* **72(3)** (2011) 443-452. <https://doi.org/10.1016/j.porgcoat.2011.06.001>
- [44] C. Verma, L. O. Olasunkanmi, E. E. Ebenso, M. A. Quraishi, *Results in Physics* **8** (2018) 657-670. <https://doi.org/10.1016/j.rinp.2018.01.008>
- [45] B. Chugh, A. K. Singh, S. Thakur, B. Pani, A. K. Pandey, H. Lgaz, I.-M. Chung, E. E. Ebenso, *Journal of Physical Chemistry C* **123(37)** (2019) 22897-22917. <https://doi.org/10.1021/acs.jpcc.9b03994>
- [46] P. Khodaei, M. I. Shabani-Nooshabadi, M. Behpour, *Progress in Organic Coatings* **136** (2019) 105254. <https://doi.org/10.1016/j.porgcoat.2019.105254>